Updating the sulcal landscape of the human lateral parieto-occipital junction provides anatomical, functional, and cognitive insights

Ethan H. Willbrand[1,2*], Yi-Heng Tsai[3*], Thomas Gagnant[4], Kevin S. Weiner[1,2**]

[1]Department of Psychology, University of California, Berkeley, Berkeley, CA, USA
[2]Helen Wills Neuroscience Institute, University of California, Berkeley, Berkeley, CA, USA
[3]Department of Psychology, University of North Carolina at Chapel Hill, Chapel Hill, NC, USA
[4]Medical Science Faculty, University of Bordeaux, Bordeaux, France
*Co-first authors
**Corresponding author: Kevin S. Weiner (kweiner@berkeley.edu)

Abstract

Understanding the tripartite relationship among neuroanatomy, brain function, and cognition is of major interest across neurobiological subdisciplines. Recent advances in neuroimaging have uncovered neuroanatomical structures in evolutionarily-expanded portions of the brain that are related to individual differences in brain function and cognition. Here, we explored this relationship in lateral parietal cortex (LPC), a region crucial for many higher-level cognitive abilities. To do so, we manually defined 2176 individual sulci across 144 hemispheres. We identified four small and shallow indentations of the cerebral cortex (sulci) that were previously unidentified in the lateral parieto-occipital junction (LPOJ) and LPC. One of these sulci (ventral supralateral occipital sulcus, slocs-v) is present in nearly every hemisphere, and is morphologically, architecturally, and functionally dissociable from neighboring sulci. Implementing a data-driven, model-based approach relating sulcal depth to behavior identified different relationships of ventral and dorsal LPC/LPOJ sulcal networks contributing to the perception of spatial orientation. The model identified the slocs-v, further indicating the importance of this new neuroanatomical structure. Our findings build on classic neuroanatomical theories and identify new neuroanatomical targets for future "precision imaging" studies exploring the relationship among brain structure, brain function, and cognitive abilities at the level of the individual participant.

Keywords

Cortical folding, Functional neuroanatomy, Magnetic resonance imaging (MRI), Occipital cortex, Parietal cortex, Spatial orientation

Introduction

A fundamental goal in neuroscience is to understand the complex relationship between brain structure and brain function, as well as how that relationship provides a scaffold for efficient cognition and behavior. Of all the neuroanatomical features to target, recent work shows that morphological features of hominoid-specific, shallow indentations, or sulci, of the cerebral cortex are not only functionally and cognitively meaningful, but also are particularly impacted by multiple brain-related disorders and aging [1–20]. The combination of these findings provides growing support for a classic theory proposing that the late emergence of these structures in gestation within association cortices, as well as their prolonged development, may co-occur with specific functional and microstructural features that could support specific cognitive abilities that also have a protracted development [21]. Nevertheless, despite the developmental, evolutionary, functional, cognitive, and theoretical relevance of these findings, they have mainly been restricted to only a subset of association cortices such as the prefrontal, cingulate, and ventral occipitotemporal cortices [1–20]. Thus, examining the relationship among these structures (also known as tertiary sulci) relative to architectonic and functional features of the cerebral cortex, as well as relative to cognition, remains uncharted in other association cortices such as the lateral parietal cortex (LPC).

As LPC is a cortical extent that has expanded extensively throughout evolution [22,23], there is great interest in the structure and function of LPC in development, aging, across species, and in different patient populations. Yet, key gaps in knowledge relating individual differences in the structure of LPC to individual differences in the functional organization of LPC and cognitive performance remain for at least four main reasons. First, one line of recent work shows that LPC displays a much more complex sulcal patterning than previously thought [24–27], while a second line of work shows that LPC is tiled with many maps and discrete functional

64   regions spanning modalities and functions such as vision, memory, attention, action, haptics,

65   and multisensory integration in addition to theory of mind, cognitive control, and subdivisions of

66   the default mode network [28–34]. Second, a majority of the time, the two lines of work are

67   conducted independently from one another and the majority of human neuroimaging studies of

68   LPC implement group analyses on average brain templates—which causes LPC sulci to

69   disappear (**figure 1**). Third, despite the recently identified complexity of LPC sulcal patterning,

70   recent studies have also uncovered previously overlooked tertiary sulci in association cortices

71   (for example, in the posterior cingulate cortex [13,15]). Thus, fourth, it is unknown if additional

72   LPC tertiary sulci are waiting to be discovered and if so, could improve our understanding of the

73   structural-functional organization of LPC with potential cognitive insights as in other association

74   cortices. Critically, while such findings would have developmental, evolutionary, functional,

75   cognitive, and theoretical implications for addressing novel questions in future studies, they

76   would also have translational applications as sulci serve as biomarkers in neurodevelopmental

77   disorders [3–6] and "corridors" for neurosurgery [35,36].

78   In the present study, we first manually defined LPC sulci in 144 young adult

79   hemispheres using the most recent definitions of LPC sulci [24]. By manually labeling over

80   2,000 sulci, we uncovered four previously undefined (Supplemental Methods and Supplemental

81   figures 1-4 for historical details) sulci in the cortical expanse between the caudal branches of the

82   superior temporal sulcus (cSTS) and two parts of the intraparietal sulcus (IPS)—a cortical

83   expanse recently referenced as containing sensory "bridge" regions of the temporal-parietal-

84   occipital junction [37]—which we term the supralateral occipital sulci (ventral: slocs-v; dorsal:

85   slocs-d) and posterior angular sulci (ventral: pAngs-d; dorsal: pAngs-d). We then utilized

86   morphological (depth and surface area), architectural (gray matter thickness and myelination),

87   and functional (resting-state functional connectivity) data available in each participant to assess

88   whether the most common of these structures (slocs-v) was dissociable from surrounding sulci.

89   Finally, we assessed whether the updated view of the LPC/LPOJ sulcal landscape provided

90   cognitive insights using a model-based, data-driven approach [17] relating sulcal morphology to

91   behavior on tasks known to activate regions within this cortical expanse (for example, reasoning

92   and spatial orientation [38–41]).

93

94   **Materials and Methods**

95   **(a) <u>Participants</u>**

96   Data for the young adult human cohort analyzed in the present study were from the Human

97   Connectome Project (HCP) database (https://www.humanconnectome.org/study/hcp-young-

98   adult/overview). Here, we used 72 participants (50% female, 22-36 years old, and 90% right-

99   handed; there was no effect of handedness on our behavioral tasks; Supplemental materials)

100   that were also analyzed in several prior studies [11–16].

101

102   **(b) <u>Neuroimaging data acquisition</u>**

103   Anatomical T1-weighted (T1-w) MRI scans (0.8 mm voxel resolution) were obtained in native

104   space from the HCP database. Reconstructions of the cortical surfaces of each participant were

105   generated using FreeSurfer (v6.0.0), a software package used for processing and analyzing

106   human brain MRI images (surfer.nmr.mgh.harvard.edu) [42,43]. All subsequent sulcal labeling

107   and extraction of anatomical metrics were calculated from these reconstructions generated

108   through the HCP's version of the FreeSurfer pipeline [44].

109

110   **(c) <u>Behavioral data:</u>**

111   In addition to structural and functional neuroimaging data, the HCP also includes a wide range

112   of behavioral metrics from the NIH toolbox [45]. To relate LPC/LPOJ sulcal morphology to

113   behavior, we leveraged behavioral data related to spatial orientation (Variable Short Penn Line

114   Orientation Test), relational reasoning (Penn Progressive Matrices Test), and processing speed

115   (Pattern Completion Processing Speed Test; Supplemental Methods for task details). We

116   selected these tasks as previous functional neuroimaging studies have shown the crucial role of

117   LPC/LPOJ in relational reasoning and spatial orientation [38–41], while our previous work

118   relating sulcal morphology to cognition uses processing speed performance as a control

119   behavioral task [17,19].

120

121   **(d) Anatomical analyses:**

122   **(i) *Manual labeling of LPC sulci***

123   Sulci were manually defined in 72 participants (144 hemispheres) guided by the most recent

124   atlas by Petrides [24], as well as recent empirical studies [25–27], which together offer a

125   comprehensive definition of cerebral sulcal patterns, including tertiary sulci. For a historical

126   analysis of sulci in this cortical expanse, please refer to Segal & Petrides [25] and Zlatkina &

127   Petrides [26]. Our cortical expanse of interest was bounded by the following sulci and gyri: (i)

128   the postcentral sulcus (PoCS) served as the anterior boundary, (ii) the superior temporal sulcus

129   (STS) served as the inferior boundary, (iii) the superior parietal lobule (SPL) served as the

130   superior boundary, and (iv) the medial and lateral transverse occipital sulci (mTOS and lTOS)

131   served as the posterior boundary. We also considered the following sulci within this cortical

132   expanse: the three different branches of the caudal superior temporal sulcus (posterior to

133   anterior: cSTS3, 2, 1), the supramarginal sulcus (SmgS), posterior intermediate parietal sulcus

134   (pips), sulcus of Brissaud (sB), anterior intermediate parietal sulcus of Jensen (aipsJ),

135   paroccipital intraparietal sulcus (IPS-PO), intraparietal sulcus (IPS), and the superior parietal

136   sulcus (SPS). Of note, the IPS-PO is the portion of the IPS extending ventrally into the occipital

137   lobe. The IPS-PO was first identified as the paroccipital sulcus by Wilder (1886). There is often

138   an annectant gyrus separating the horizontal portion of the IPS proper from the IPS-PO [26,46].

139   Additionally, we identified as many as four previously uncharted and variable tertiary

140   LPC/LPOJ sulci for the first time: the supralateral occipital sulcus (slocs; composed of ventral

141   (slocs-v) and dorsal (slocs-d) components) and the posterior angular sulcus (pAngs; composed

142   of ventral (pAngs-v) and dorsal (pAngs-d) components). In the Supplemental Methods and

143   Supplemental Figures 1-4, we discuss the slocs and pAngs within the context of modern and

144   historical sources.

145   For each participant in each hemisphere, the location of each sulcus was confirmed by

146   trained independent raters (E.H.W., Y.T., and T.G.) and finalized by a neuroanatomist (K.S.W.).

147   All LPC sulci were then manually defined in FreeSurfer using tksurfer tools, as in previous work

148   [11–20], from which morphological and anatomical features were extracted. For four example

149   hemispheres with these 13-17 sulci identified, see **figure 1a** (Supplemental figure 5 for all

150   hemispheres). The specific criteria to identify the slocs and pAngs are outlined in **figure 1b**. We

151   also generated sulcal probability maps for each sulcus (Supplemental Methods and

152   Supplemental figure 6).

153   To test whether the incidence rates of the slocs and pAngs components were statistically

154   different, we implemented a binomial logistic regression GLM with sulcus (slocs-v, slocs-d,

155   pAngs-v, and pAngs-d) and hemisphere (left and right), as well as their interaction, as predictors

156   for sulcal presence [0 (absent), 1 (present)]. GLMs were carried out with the glm function from

157   the built-in stats R package. ANOVA χ2 tests were applied to each GLM with the Anova function

158   from the car R package, from which results were reported.
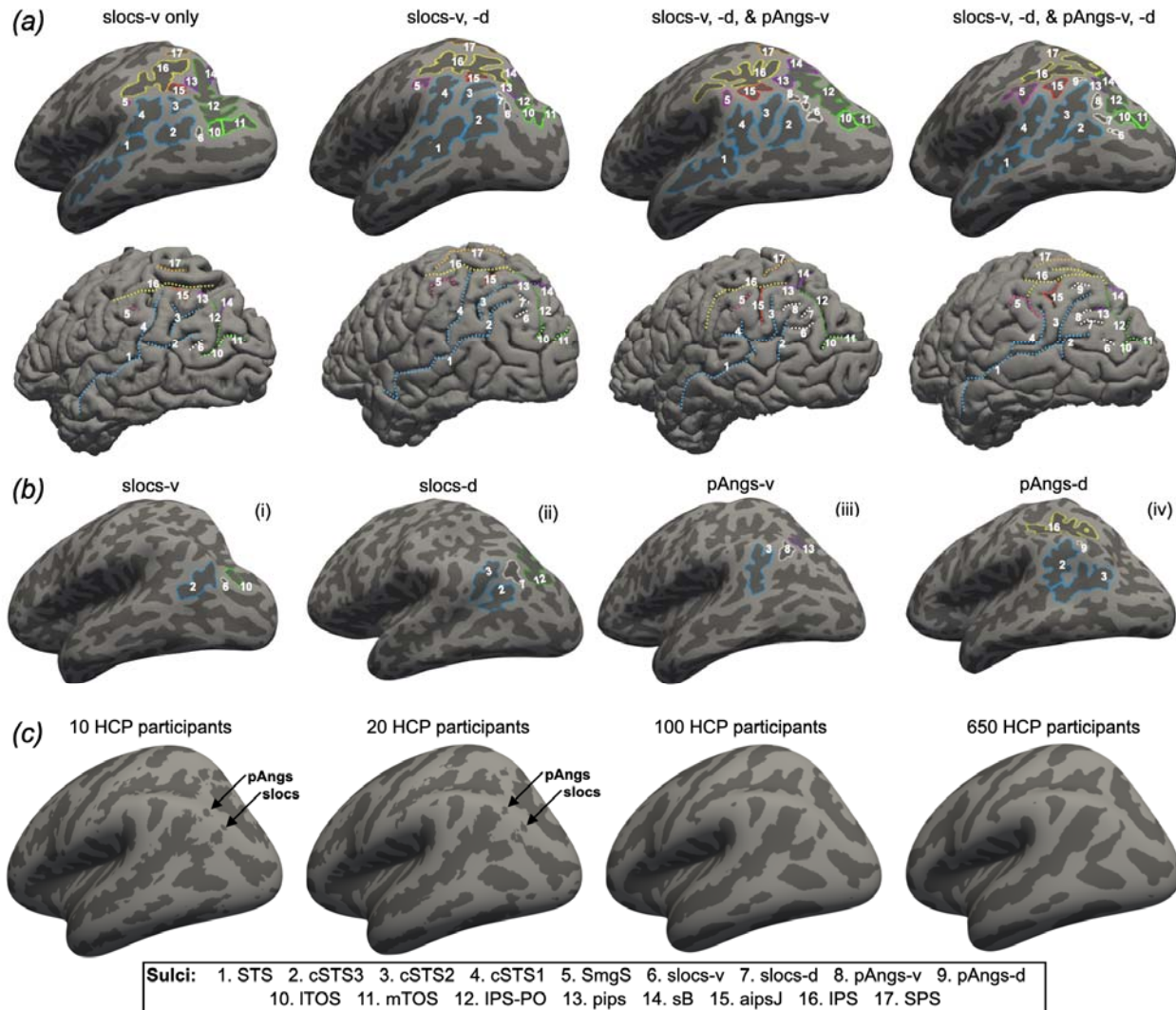
Figure 1. Four previously undefined small and shallow sulci in the lateral parieto-occipital junction (LPOJ). *(a)* Four example inflated (top) and pial (bottom) left hemisphere cortical surfaces displaying the 13-17 sulci manually identified in the present study. Each hemisphere contains 1-4 of the previously undefined and variable LOC/LPOJ sulci (slocs and pAngs). Each sulcus is numbered according to the legend. *(b)* Criteria for defining slocs and pAngs components. (i) Slocs-v is the cortical indentation between the cSTS3 and ITOS. (ii) Slocs-d is the indentation between cSTS3/cSTS2 and IPS-PO. (iii) pAngs-v is the indentation between the cSTS2 and pips. (iv) pAngs-d is the indentation between cSTS2/cSTS1 and IPS. *(c)* The variability of the slocs and pAng components can cause them to disappear when individual surfaces are averaged together. Left to right: (i) 10 HCP participants, (ii) 20 HCP participants, (iii) 100 HCP participants, and iv) 650 HCP participants. The disappearance of these sulci on average surfaces, which are often used for group analyses in neuroimaging research, emphasizes the importance of defining these structures in individual hemispheres.

173 **(ii) *Extracting and comparing the morphological and architectural features from sulcal***

174 ***labels***

175 Morphologically, we compared sulcal depth and surface area across sulci, as these are two of

176 the primary morphological features used to define and characterize sulci [8,10–13,16–18,21,47–

177 51]. As in our prior work [17,18], mean sulcal depth values (in standard FreeSurfer units) were

178 computed in native space from the .sulc file generated in FreeSurfer [42] with custom Python

179 code [17]. Briefly, depth values are calculated based on how far removed a vertex is from what

180 is referred to as a "mid-surface," which is determined computationally so that the mean of the

181 displacements around this "mid-surface" is zero. Thus, generally, gyri have negative values,

182 while sulci have positive values. Each depth value was also normalized by the deepest point in

183 the given hemisphere. Surface area (mm^2) was calculated with the FreeSurfer

184 mris_anatomical_stats function

185 (https://surfer.nmr.mgh.harvard.edu/fswiki/mris_anatomical_stats). The morphological features

186 of all LPC/LPOJ sulci are documented in Supplemental figure 7.

187 Architecturally, we compared cortical thickness and myelination, as in our prior work in

188 other cortical expanses [12,13,16,17]. Mean gray matter cortical thickness (mm) was extracted

189 using the FreeSurfer mris_anatomical_stats function. To quantify myelin content, we used the

190 T1-w/T2-w maps for each hemisphere, an in vivo myelination proxy [52]. To generate the T1-

191 w/T2-w maps, two T1-w and T2-w structural MR scans from each participant were registered

192 together and averaged as part of the HCP processing pipeline [44]. The averaging helps to

193 reduce motion-related effects or blurring. Additionally, and as described by Glasser and

194 colleagues [44], the T1-w/T2-w images were bias-corrected for distortion effects using field

195 maps. We then extracted the average T1-w/T2-w ratio values across each vertex for each

196 sulcus using custom Python code [12]. The architectural features of all LPC/LPOJ sulci are

197 documented in Supplemental figure 7.

198   To assess whether these four metrics differed between the slocs-v and surrounding sulci

199   (cSTS3 and lTOS), we ran a repeated measure analysis of variance (rm-ANOVA) with the

200   within-participant effects of sulcus (slocs-v, cSTS3, and lTOS), metric (surface area, depth,

201   cortical thickness, and myelination), and hemisphere (left and right). Rm-ANOVAs (including

202   sphericity correction) were implemented with the aov_ez function from the afex R package.

203   Effect sizes for the ANOVAs are reported with the partial eta-squared metric (η2). Post-hoc

204   analyses were computed with the emmeans function from the emmeans R package (*p*-values

205   corrected with Tukey's method). We also repeated these analyses for the three cSTS

206   components [24,25] and the two intermediate parietal sulcal components (ips: aipsJ and pips

207   [24,26]; detailed in the Supplemental Results and Supplemental Figure 8) as these components,

208   to our knowledge, have not been quantitatively compared in previous work.

209   **(f) <u>Functional analyses</u>**

210   To determine if the slocs-v is functionally distinct from surrounding sulci, we generated

211   functional connectivity profiles using recently developed analyses [12,13,53]. First, we used

212   resting-state network parcellations for each individual participant from Kong and colleagues [54],

213   who generated individual network definitions by applying a hierarchical Bayesian network

214   algorithm to produce maps for each of the 17 networks in individual HCP participants.

215   Importantly, this parcellation was conducted blind to both cortical folding and our sulcal

216   definitions. Next, we resampled the network profiles for each participant onto the fsaverage

217   cortical   surface,   and   then   to   each   native   surface   using   CBIG   tools

218   (https://github.com/ThomasYeoLab/CBIG). We then calculated the spatial overlap between a

219   sulcus and each of the 17 individual resting-state networks via the Dice coefficient (Equation 1):

220    $$(1) \quad Dice\,(\square, \square) \;=\; \frac{2\,|\square \cap \square|}{|\square| + |\square|}$$

221   This process of calculating the overlap between each sulcus and the 17-network

222   parcellation generated a "connectivity fingerprint" for each sulcus in each hemisphere of each

223   participant. We then ran an rm-ANOVA with within-participant factors of sulcus (slocs-v, cSTS3,

224   and ITOS), network (17 networks), and hemisphere (left and right) to determine if the network

225   profiles (i.e., the Dice coefficient overlap with each network) of the slocs-v was differentiable

226   from the surrounding sulci (i.e., cSTS3 and ITOS). Here we discuss effects related to networks

227   that at least showed minor overlap with one sulcus (i.e., Dice ≥ .10). As in the prior analysis, we

228   also repeated these analyses for the three cSTS components and the two intermediate parietal

229   sulcal components (Supplemental Results and Supplemental Figure 8).

230

231   **(g)** **Behavioral analyses**

232   **(i)** *Model selection*

233   The analysis relating sulcal morphology to spatial orientation and/or reasoning consisted of

234   using a cross-validated least absolute shrinkage and selection operator (LASSO) regression to

235   select the sulci that explained the most variance in the data and determined how much variance

236   is explained by sulcal depth as a predictor of behavior, as implemented in our previous work

237   [16–18]. The depths of all LPC/LPOJ sulci were included as predictors in the LASSO regression

238   model (Supplemental Methods for details on demographic control variables). As the shrinkage

239   parameter (alpha) increases, it decreases the coefficient of each of the sulci to zero except for

240   those with the strongest association. Therefore, this technique highlights the sulci whose

241   morphology was most closely related to behavior. We used cross-validation to optimize the

242　　shrinking parameter for the LASSO regression. Conventionally, we selected the model

243　　parameters that minimized the cross-validated mean squared error (MSE_{cv}) [55]. The

244　　optimization was performed with the GridSearchCV function sklearn in Python, which allowed us

245　　to determine the model parameters minimizing the MSE_{cv}. To evaluate the performance of any

246　　model selected by the LASSO regression, as in prior work [16–18], we measured the model

247　　performance for the relevant behavioral task using nested model comparison. With leave-one-

248　　out cross-validation (LooCV), we compared the LASSO-selected model with the predictors to a

249　　model with all left hemisphere sulci as predictors.

250

251　　**(ii) *Assessing morphological and behavioral specificity***

252　　To assess whether our findings generalized to other anatomical features, we considered cortical

253　　thickness, which is consistently studied in cognitive neuroscience studies relating morphology to

254　　cognition [16–18,56,57]. To do so, we replaced sulcal depth with cortical thickness as the

255　　predictive metric in our LASSO-selected model. As with depth, the model was fit to the data with

256　　LooCV. To compare the thickness model to the depth model, we used the Akaike Information

257　　Criterion (AIC), which provides an estimate of in-sample prediction error and is suitable for non-

258　　nested model comparison. By comparing AIC scores, we are able to assess the relative

259　　performance of the two models. If the ΔAIC is > 2, it suggests an interpretable difference

260　　between models. If the ΔAIC is > 10, it suggests a strong difference between models, with the

261　　lower AIC value indicating the preferred model [58]. To also ascertain whether the relationship

262　　between LPC/LPOJ sulcal depth and cognition is specific to spatial orientation performance, or

263 transferable to other general measures of cognitive processing, we investigated the

264 generalizability of the sulcal-behavior relationship to another widely used measure of cognitive

265 functioning: processing speed [59]. Specifically, we used LooCV to predict processing speed

266 instead of spatial orientation score. As with thickness, we compared the two models with the

267 AIC.

268

269 **Results**

270 **(a) <u>Four previously undefined small and shallow sulci in the lateral parieto-occipital</u>**

271 **<u>junction (LPOJ)</u>**

272 In addition to defining the 13 sulci previously described within the LPC/LPOJ, as well as the

273 posterior superior temporal cortex (**Materials and Methods**) [24] in individual participants, we

274 could also identify as many as four small and shallow sulci situated within the LPC/LPOJ that

275 were more variable across individuals and uncharted until now (Supplemental Methods and

276 Supplemental figures 1-4). Macroanatomically, we could identify two sulci between the cSTS3

277 and the IPS-PO/ITOS ventrally and two sulci between the cSTS2 and the pips/IPS dorsally.

278 Ventrally, we refer to these sulci as ventral (slocs-v; sulcus 5 in **figure 1**) and dorsal

279 (slocs-d; sulcus 6 in **figure 1**) components of the supralateral occipital sulcus. The slocs-v,

280 located between the posterior cSTS3 and ITOS, was present in 98.6% of hemispheres (left

281 hemisphere: N = 71/72; right hemisphere: N = 71/72; **figure 1**). Conversely, the slocs-d, located

282 between the cSTS3 and IPS-PO, was present 68.0% of the time (left hemisphere: N = 50/72;

283 right hemisphere: N = 48/72; **figure 1**). Dorsally, we refer to the other newly identified sulci as

284 the ventral (pAngs-v; sulcus 7 in **figure 1**) and dorsal (pAngs-d; sulcus 8 in **figure 1**)

285 components of the posterior angular sulcus. The pAng components were more rare than the

286 slocs components. Specifically, pAngs-v, located between cSTS2 and pips, was identifiable

287 31.3% of the time (19 left and 26 right hemispheres; **figure 1**). Located between cSTS2 and the

288   IPS, pAngs-d was identifiable only 13.2% of the time (8 left and 11 right hemispheres; **figure 1**).

289   Though we characterize these sulci in this paper for the first time, the location of these four sulci

290   is consistent with the presence of variable "accessory sulci" in this cortical expanse mentioned

291   in prior modern and classic studies (Supplemental Methods).

292   These incidence rates were significantly different (GLM, main effect of sulcus:

293   $\chi2(3)\square=\square166.53$, $p < .0001$; no hemispheric effects: ps > .68). The slocs-v was more common

294   than the other three sulci (ps < .0001), slocs-d was more common than the pAngs components

295   (ps < .0001), and pAngs-v was more common than pAngs-d ($p = .002$). We could further identify

296   these sulci in post-mortem hemispheres (Supplemental figures 2, 3). Finally, to help guide future

297   research on these newly- and previously-classified LPC/LPOJ sulci, we generated probabilistic

298   maps of each of these 17 sulci and share them with the field with the publication of this paper

299   (Supplemental figure 6; **Data accessibility statement**).

300

301   **(b) The slocs-v is morphologically, architecturally, and functionally dissociable from**

302   **nearby sulci**

303   Given that the slocs-v was present in the majority of participants (98.6% across hemispheres),

304   we focused our analyses on this stable sulcal feature of the LPOJ. To do so, we first tested

305   whether the slocs-v was morphologically (depth and surface area) and architecturally (gray

306   matter thickness and myelination) distinct from the two sulci surrounding it: the cSTS3 and ITOS

307   (**figure 1**; Supplemental figure 7 for these metrics in all 17 sulci examined). An rm-ANOVA

308   (within-participant factors: sulcus, metric, and hemisphere for standardized metric units)

309   revealed a sulcus x metric interaction ($F(4, 276.19) = 179.15$, $\eta2 = 0.38$, $p < .001$). Post hoc

310   tests showed four main differences: (i) the slocs-v was shallower than cSTS3 ($p < .001$) but not

311   ITOS ($p = .60$), (ii) the slocs-v was smaller than both the cSTS3 and ITOS (ps < .001), (iii) the

312   slocs-v was thicker than both the cSTS3 and ITOS (ps < .001), and iv) the slocs-v was less

bioRxiv preprint doi: https://doi.org/10.1101/2023.06.08.544284; this version posted June 9, 2023. The copyright holder for this preprint (which was not certified by peer review) is the author/funder, who has granted bioRxiv a license to display the preprint in perpetuity. It is made available under aCC-BY-NC 4.0 International license.

313   myelinated than both the cSTS and ITOS (ps < .001; **figure 2a**). There was also a sulcus x

314   metric x hemisphere interaction ($F(4.20, 289.81) = 4.16$, η2 = 0.01, p = .002; Supplemental

315   Results).

316   We then tested whether the slocs-v was also functionally distinct from the cSTS3 and

317   ITOS by leveraging resting-state network parcellations for each individual participant to quantify

318   "connectivity fingerprints" for each sulcus in each hemisphere of each participant (**Materials**

319   **and Methods**) [54]. An rm-ANOVA (within-participant factors: sulcus, network, and hemisphere

320   for Dice coefficient overlap) revealed a sulcus x network interaction ($F(32, 2144) = 80.18$, η2 =

321   0.55, p < .001). Post hoc tests showed that this interaction was driven by four effects: (i) the

322   cSTS3 overlapped more with the Default A subnetwork than both the slocs-v and ITOS (ps <

323   .001), (ii) the slocs-v overlapped more with the Default C subnetwork than the ITOS (p < .001)

324   and marginally than the cSTS3 (p = .077), (iii) the slocs-v overlapped more with the Dorsal

325   Attention A subnetwork than both the cSTS3 and ITOS (ps < .001), and iv) the ITOS overlapped

326   more with the Visual A and Visual B subnetworks than both the cSTS3 and slocs-v (ps < .004;

327   **figure 2b**). There was also a sulcus x network x hemisphere interaction ($F(32, 2144) = 3.99$, η2

328   = 0.06, p < .001; Supplemental Results). Together, these results indicate that the slocs-v is a

329   morphologically, architecturally, and functionally distinct structure from its sulcal neighbors, and

330   thus, deserves a distinct neuroanatomical definition.

331   We further found that the three caudal STS rami [24,25] and intermediate parietal sulci

332   (aipsJ and pips) [24,26] are morphologically, architecturally, and functionally distinct structures

333   for the first time (to our knowledge), which empirically supports their distinctions with separate

334   sulcal labels (Supplemental Results and Supplemental figure 8).

335

336
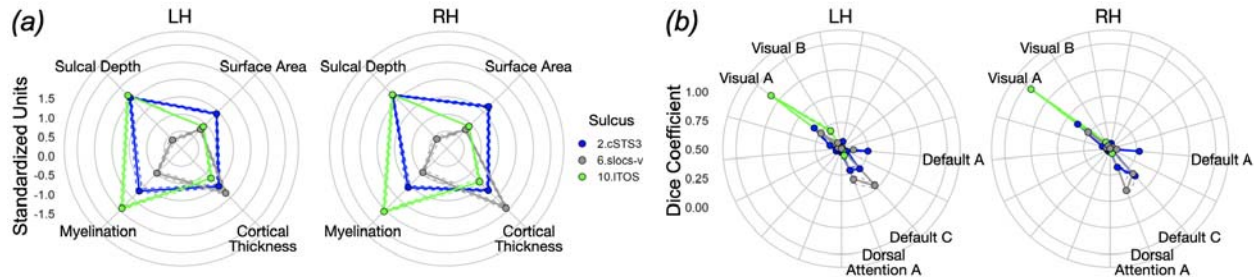
Figure 2. The slocs-v is morphologically, architecturally, and functionally dissociable from nearby sulci. *(a)* Radial plot displaying the morphological (upper metrics: depth, surface area) and architectural (lower metrics: cortical thickness, myelination) features of the slocs-v (gray), cSTS3 (blue), and lTOS (green). Each dot and solid line represent the mean. The dashed lines indicate ± standard error. These features are colored by sulcus (legend). Metrics are in standardized units. *(b)* Radial plot displaying the connectivity fingerprints of these three sulci: the Dice Coefficient overlap (values from 0-1) between each component and individual-level functional connectivity parcellations [54].

(c) The morphology of LPC/LPOJ sulci, including the slocs-v, is related to cognitive performance

Finally, leveraging a data-driven approach of cross-validated LASSO feature selection, we sought to determine whether sulcal depth, a main defining feature of sulci, related to cognitive performance (**Materials and Methods**). To do so, we primarily focused on spatial orientation and reasoning given that these abilities recruit multiple subregions of lateral parietal and/or occipital cortices [38–41]. As in prior work [16–18], we chose the model at the alpha that minimized MSE_{cv}. Participants with a slocs-v in both hemispheres and all behavioral metrics were included (N = 69). Due to their rarity (being in less than 70% of hemispheres at most), we did not include the slocs-d or pAng components in this analysis.

This method revealed an association between spatial orientation scores and normalized sulcal depth in the left hemisphere (MSE_{cv} = 25.63, alpha = 0.05; **figure 3a**), but not in the right hemisphere (MSE_{cv} = 26.41, alpha = 0.3). Further, we found that no LPC/LPOJ sulci were selected for reasoning in either hemisphere (right*:* alpha = 0.3, MSE = 24.01; left: alpha = 0.3, MSE = 24.01). Six left hemisphere LPC/LPOJ sulci were related to spatial orientation task

361   performance **figure 3a, b**). Four of these sulci were positioned ventrally: cSTS3 (β = -9.77),

362   slocs-v (β = -3.36), lTOS (β = -4.91), and mTOS (β = -0.06), whereas two were positioned

363   dorsally: pips (β = 5.02), and SPS (β = 4.30; **figure 3a, b**). Using LooCV to construct models

364   that predict behavior, the LASSO-selected model explained variation in spatial orientation score

365   (R^2_{cv} = 0.06, MSE_{cv} = 23.99) above and beyond a model with all left hemisphere sulci (R^2_{cv} <

366   0.01, MSE_{cv} = 27.12). This model also showed a moderate correspondence (r_s = 0.29, p = .01;

367   **figure 3c**) between predicted and actual measured scores. We then tested for anatomical and

368   behavioral specificity using the AIC, which revealed two primary findings. First, we found that

369   the LASSO-selected sulcal depth model outperformed a model using the cortical thickness of

370   the six LASSO-selected sulci (R^2_{cv} < .01, MSE_{cv} = 26.02, $AIC_{cortical\ thickness} - AIC_{sulcal\ depth}$ = 2.19).

371   This model also showed task specificity as these sulci outperformed a model with processing

372   speed (R^2_{cv} < .01, MSE_{cv} = 254.65, $AIC_{processing\ speed} - AIC_{spatial\ orientation}$ = 63.57). Thus, our data-

373   driven model explains a significant amount of variance on a spatial orientation task and shows

374   behavioral and morphological specificity.

375

376
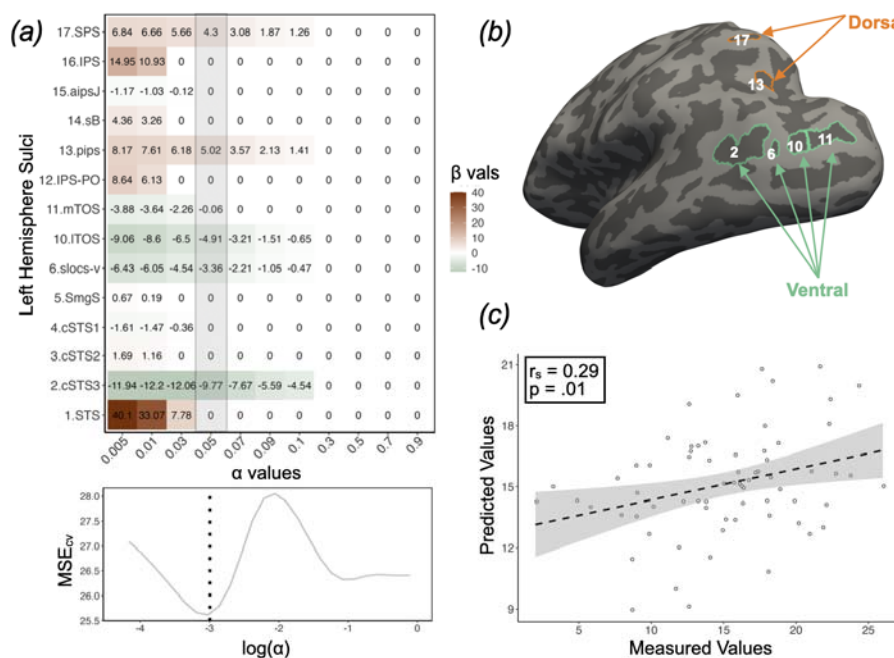
Figure 3. The morphology of LPC/LPOJ sulci, including the slocs-v, is related to cognitive performance. *(a)* Beta-coefficients for each left hemisphere LPC/LPOJ sulcus at a range of shrinking parameter values [alpha (α)]. Highlighted gray bar indicates coefficients at the chosen α-level. Bottom: Cross-validated mean-squared error

393 (MSE$_{CV}$) at each α level. By convention, we selected the α that minimized the MSE$_{CV}$ (dotted line). *(b)*

394 Inflated left hemisphere cortical surface from an example participant highlighting the two groups of sulci—

395 *dorsal positive* (orange) and *ventral negative* (green)—related to spatial orientation performance. *(c)*

396 Spearman's correlation (r$_s$) between the measured and the predicted spatial orientation scores from the

397 LASSO-selected model is shown in *(a)*.

398

399 **Discussion**

400 **(a) <u>Overview</u>**

401 In the present study, we examined the relationship between LPC/LPOJ sulcal morphology,

402 functional connectivity fingerprints, and cognition. We report five main findings. First, while

403 manually defining sulci in LPC/LPOJ across 144 hemispheres, we uncovered four new small

404 and shallow sulci that are not included in present or classic neuroanatomy atlases or

405 neuroimaging software packages. Second, we found that the most common of these structures

406 (the slocs-v; identifiable 98.6% of the time) was morphologically, architecturally, and functionally

407 differentiable from nearby sulci. Third, using a model-based, data-driven approach quantifying

408 the relationship between sulcal morphology and cognition, we found a relationship between the

409 depths of six LPC/LPOJ sulci and performance on a spatial orientation processing task. Fourth,

410 the model identified distinct dorsal and ventral sulcal networks in LPC/LPOJ: ventral sulci had

411 negative weights while dorsal sulci had positive weights (**figure 3*b***). These findings are

412 consistent with previous neuroimaging work from Gur et al. [41] who demonstrated separate

413 functional activations in dorsal parietal and the more ventrally situated occipital-parietal cortices

414 for the judgment of line orientation task used in the present study. Fifth, the model identified that

415 the slocs-v is cognitively relevant, further indicating the importance of this new neuroanatomical

416 structure. In the sections below, we discuss (i) the slocs-v relative to modern functional and

417 cytoarchitectonic parcellations in the LPC/LPOJ, as well as anatomical connectivity to other

418 parts of the brain, (ii) underlying anatomical mechanisms relating sulcal morphology and

419   behavior more broadly, and (iii) limitations of the present study. Implications for future studies

420   are distributed throughout each section.

421

422   **(b) The slocs-v relative to modern functional and cytoarchitectonic parcellations in the**

423   **LPC/LPOJ, as well as anatomical connectivity to other parts of the brain**

424   To lay the foundation for future studies relating the newly-identified slocs-v to different

425   anatomical and functional organizational features of LPC/LPOJ, we situate probabilistic

426   predictions of slocs-v relative to probabilistic cortical areas identified using multiple modalities.

427   For example, when examining the correspondence between the slocs-v and modern multimodal

428   (HCP-MMP [37]) and observer-independent cytoarchitectural (Julich-Brain atlas [60]) areas

429   (Supplemental Methods), the slocs-v is located within distinct areas. In particular, the slocs-v

430   aligns with the multimodally- and cytoarchitecturally-defined area PGp bilaterally and

431   cytoarchitecturally-defined hIP4 in the right hemisphere (**figure 4**). In classic neuroanatomical

432   terms [61], this indicates that the slocs-v is a putative "axial sulcus" for these regions, which

433   future work can assess with analyses in individual participants.

434
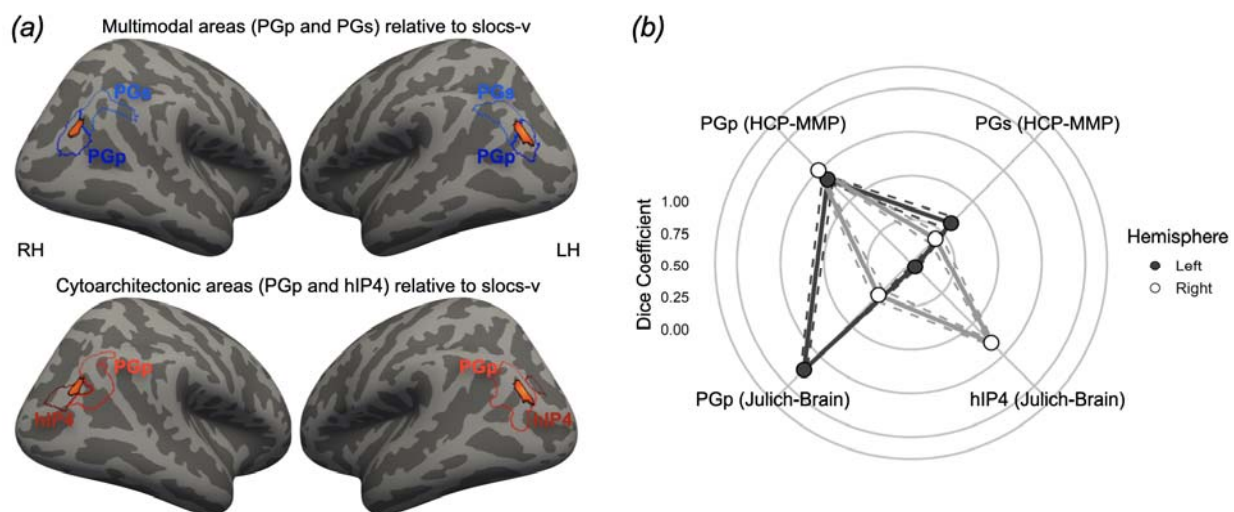
435

436 **Figure 4. The slocs-v relative to modern functional and cytoarchitectonic parcellations in**
437 **LPC/LPOJ.** *(a)* Top: Left (LH) and right (RH) hemispheres of the inflated fsaverage surface with two
438 areas from the modern HCP multimodal parcellation (HCP-MMP; blue) [37] relative to an MPM of the
439 slocs-v (warm colors indicate areas with at least 20% overlap across participants; Supplemental figure 6).
440 Bottom: Same as top, except for two observer-independent cytoarchitectonic regions from the Julich-
441 Brain Atlas [60]. *(b)* Overlap between the slocs-v and each area (Supplemental Methods). Each dot and
442 solid line represents the mean. The dashed lines indicate ± standard error (left: gray; right: white).
443

444   Aside from recent multimodal and observer-independent cytoarchitectonic parcellations,

445 an immediate question is: What is the relationship between the slocs-v and other functional

446 regions at this junction between the occipital and parietal lobes, as well as potential anatomical

447 connectivity? For example, there are over a dozen visual field maps in the cortical expanse

448 spanning the TOS, IPS-PO, and the IPS proper (see (i), (ii), and (iii), respectively in **figure 5*a***)

449 [33]. When projecting probabilistic locations of retinotopic maps from over 50 individuals from

450 Wang and colleagues [62] (Supplemental Methods), the slocs-v is likely located outside of visual

451 field maps extending into this cortical expanse (**figure 5*a***). Nevertheless, when also projecting

452 the map of the mean R^2 metric from the HCP retinotopy dataset from 181 participants shared by

453 Benson and colleagues [63] (Supplemental Methods), the slocs-v is in a cortical expanse that

454 explains a significant amount of variance (left hemisphere: R^2_{mean} = 19.29, R^2_{max} = 41.73; right

455 hemisphere: R^2_{mean} = 21.17, R^2_{max} = 44.23; **figure 5*b***).

456

457
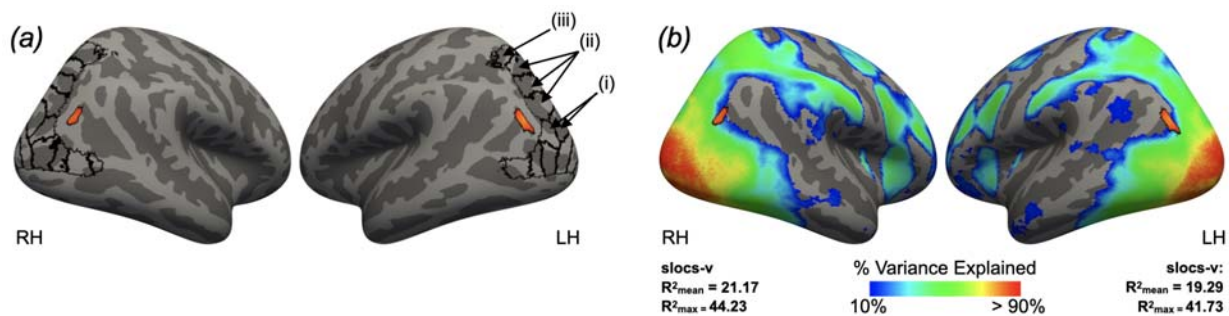
458

459 **Figure 5. The slocs-v relative to retinotopy.** *(a)* Top: Left (LH) and right (RH) hemispheres of the
460 inflated fsaverage surface displaying the probabilistic locations of retinotopic maps from over 50
461 individuals from Wang and colleagues [62] (black outlines). The predicted slocs-v location from the MPMs
462 is overlaid in orange (as in figure 4). (i), (ii), and (iii) point out the retinotopic maps in the cortical expanse
463 spanning the TOS, IPS-PO, and IPS, respectively. *(b)* Same format as in *(a)*, but with a map of the mean
464 R^2 metric from the HCP retinotopy dataset [63] overlaid on the fsaverage surfaces (thresholded
465 between R^2 values of 10% and 90%). This metric measures how well the fMRI time series at each vertex
466 is explained by a population receptive field (pRF) model. The mean and max R^2 values for the slocs-v
467 MPM in each hemisphere are included below each surface.

468

469   In terms of anatomical connectivity, as the slocs-v co-localizes with cytoarchitectonically

470 defined PGp (**figure 4**) and previous studies have examined the anatomical connectivity of the

471 probabilistically defined PGp, we can glean insight regarding the anatomical connectivity of

472 slocs-v from these previous studies [64,65]. This prior work showed that PGp was anatomically

473 connected to temporooccipital regions, other regions in the temporal lobe, middle and superior

474 frontal cortex, as well as the inferior frontal cortex and insula [64,65]. Of course, the location of

475 the slocs-v relative to multimodal, cytoarchitectonic, and retinotopic areas, as well as the

476 anatomical connectivity of the slocs-v, would need to be examined in individual participants, but

477 the present work makes clear predictions for future studies as fleshed out here. To conclude this

478 section, as the multimodal area PGp (**figure 4**) was recently proposed as a "transitional area"

479 by Glasser and colleagues [37] (Supplemental table 1), future studies can also further

480 functionally and anatomically test the transitional properties of slocs-v.

481

482 **(c) Underlying anatomical mechanisms relating sulcal morphology and behavior**

483 In this section, we discuss potential anatomical mechanisms contributing to the relationship

484 between sulcal depth and behavior in two main ways. First, long-range white matter fibers have

485 a gyral bias, while short-range white matter fibers have a sulcal bias in which some fibers

486 project directly from the deepest points of a sulcus [66–70]. As such, recent work hypothesized

487 a close link between sulcal depth and short-range white matter properties [16–18,71,72]: deeper

488 sulci would reflect even shorter short-range white matter fibers, which would result in faster

489 communication between local, cortical regions and in turn, contribute to improved cognitive

490 performance. This increased neural efficiency could underlie individual differences in cognitive

491 performance. Ongoing work is testing this hypothesis which can be further explored in future

492 studies incorporating anatomical, functional, and behavioral measures, as well as computational

493 modeling.

494 Second, our model-based approach identified separate dorsal and ventral sulcal

495 networks in which deeper sulci dorsally and shallower sulci ventrally contributed to the most

496 explained variance on the spatial orientation task. A similar finding was identified by our

497 previous work in the lateral prefrontal cortex [18]. These previous and present findings may be

498 explained by the classic anatomical compensation theory, which proposes that the size and

499 depth of a sulcus counterbalance those of the neighboring sulci [23,48,73]. Thus, a larger,

500 deeper sulcus would be surrounded by sulci that are smaller and shallower, rendering the

501 overall degree of cortical folding within a given region approximately equal [23,48,73]. Future

502 work can incorporate underlying white matter architecture into the compensation theory, as well

503 as a recent modification that proposed to also incorporate local morphological features such as

504 the deepest sulcal point (e.g., sulcal pit or sulcal root [74]), which has recently been shown to be

505 related to different functional features of the cerebral cortex [50,51,75]. Altogether, these and

506 recent findings begin to build a multimodal mechanistic neuroanatomical understanding

507 underlying the complex relationship between sulcal depth and cognition relative to other

508 anatomical features.

509

510 **(d) Limitations**

511 The main limitation of our study is that presently, the most accurate methodology to define sulci

512 —especially the small, shallow, and variable tertiary sulci—requires researchers to manually

513   trace each structure on the cortical surface reconstructions. This method is arduous and time-

514   consuming, which, on the one hand, limits the sample size in terms of number of participants,

515   while on the other, results in thousands of precisely defined sulci - a push-pull relationship

516   reflecting a conversation in the broader human brain mapping and cognitive neuroscience fields

517   between a balance of large N studies and "precision imaging" studies in individual participants

518   [76–79]. Though our sample size is comparable to other studies that produced reliable results

519   relating sulcal morphology to brain function and cognition (e.g., [3,4,8,10,12,13,17–19,46]),

520   ongoing work that uses deep learning algorithms to automatically define sulci should result in

521   much larger sample sizes in future studies [80,81]. Finally, the time-consuming manual

522   definitions of primary, secondary, and tertiary sulci also limit the cortical expanse explored in

523   each study, thus, restricting the present study to LPC/LPOJ.

524

525   **(e) Conclusion**

526   In conclusion, we uncovered four previously-undefined sulci in LPC/LPOJ and quantitatively

527   showed that the slocs-v is a stable sulcal landmark that is morphologically, architecturally, and

528   functionally differentiable from surrounding sulci. We further used a data-driven, model-based

529   approach relating sulcal morphology to behavior, which identified different relationships of

530   ventral and dorsal LPC/LPOJ sulcal networks contributing to the perception of spatial

531   orientation. The model identified the slocs-v, further indicating the importance of this new

532   neuroanatomical structure. Altogether, this work provides a scaffolding for future "precision

533   imaging" studies interested in understanding how anatomical and functional features of

534   LPC/LPOJ relate to cognitive performance at the individual level.

Ethics statement

Human participants: HCP consortium data were previously acquired using protocols approved by the Washington University Institutional Review Board (Mapping the Human Connectome: Structure, Function, and Heritability; IRB # 201204036). Informed consent was obtained from all participants. The data are treated according to the WU-Minn HCP Consortium data use terms and the terms of use for the restricted data.

Competing interests statement

The authors declare no competing financial interests.

Data accessibility statement

The processed and anonymized HCP neuroimaging data required to perform all statistical analyses and reproduce all figures used for this project are available on GitHub (https://github.com/cnl-berkeley/stable_projects/tree/main/Updating_LPOJ_sulci) and Dryad (DOI: doi:10.5061/dryad.rbnzs7hh9) repositories. The analysis pipelines are available on Open Science Framework (https://osf.io/7fwqk/).

Acknowledgments

Funding information

References

1. Amiez C, Wilson CRE, Procyk E. 2018 Variations of cingulate sulcal organization and link with cognitive performance. *Sci. Rep.* **8**, 1–13. (doi:10.1038/s41598-018-32088-9)

2. Amiez C, Sallet J, Hopkins WD, Meguerditchian A, Hadj-Bouziane F, Ben Hamed S, Wilson CRE, Procyk E, Petrides M. 2019 Sulcal organization in the medial frontal cortex provides insights into primate brain evolution. *Nat. Commun.* **10**, 1–14. (doi:10.1038/s41467-019-11347-x)

3. Cachia A, Borst G, Jardri R, Raznahan A, Murray GK, Mangin J-F, Plaze M. 2021 Towards Deciphering the Fetal Foundation of Normal Cognition and Cognitive Symptoms From Sulcation of the Cortex. *Front. Neuroanat.* **15**, 712862. (doi:10.3389/fnana.2021.712862)

4. Garrison JR, Fernyhough C, McCarthy-Jones S, Haggard M, Australian Schizophrenia Research Bank, Simons JS. 2015 Paracingulate sulcus morphology is associated with hallucinations in the human brain. *Nat. Commun.* **6**, 8956. (doi:10.1038/ncomms9956)

5. Nakamura M, Nestor PG, Shenton ME. 2020 Orbitofrontal Sulcogyral Pattern as a Transdiagnostic Trait Marker of Early Neurodevelopment in the Social Brain. *Clin. EEG Neurosci.* **51**, 275–284. (doi:10.1177/1550059420904180)

6. Ammons CJ, Winslett M-E, Bice J, Patel P, May KE, Kana RK. 2021 The mid-fusiform sulcus in autism spectrum disorder: Establishing a novel anatomical landmark related to face processing. *Autism Res.* **14**, 53–64. (doi:10.1002/aur.2425)

7. Fornito A, Yücel M, Wood S, Stuart GW, Buchanan J-A, Proffitt T, Anderson V, Velakoulis D, Pantelis C. 2004 Individual differences in anterior cingulate/paracingulate morphology are related to executive functions in healthy males. *Cereb. Cortex* **14**, 424–431. (doi:10.1093/cercor/bhh004)

8. Lopez-Persem A, Verhagen L, Amiez C, Petrides M, Sallet J. 2019 The Human Ventromedial Prefrontal Cortex: Sulcal Morphology and Its Influence on Functional Organization. *J. Neurosci.* **39**, 3627–3639. (doi:10.1523/JNEUROSCI.2060-18.2019)

9. Harper L *et al.* 2022 Prenatal Gyrification Pattern Affects Age at Onset in Frontotemporal Dementia. *Cereb. Cortex* (doi:10.1093/cercor/bhab457)

10. Weiner KS. 2019 The Mid-Fusiform Sulcus (sulcus sagittalis gyri fusiformis). *Anat. Rec.* **302**, 1491–1503. (doi:10.1002/ar.24041)

11. Miller JA, Voorhies WI, Li X, Raghuram I, Palomero-Gallagher N, Zilles K, Sherwood CC, Hopkins WD, Weiner KS. 2020 Sulcal morphology of ventral temporal cortex is shared between humans and other hominoids. *Sci. Rep.* **10**, 17132. (doi:10.1038/s41598-020-73213-x)

12. Miller JA, Voorhies WI, Lurie DJ, D'Esposito M, Weiner KS. 2021 Overlooked Tertiary Sulci Serve as a Meso-Scale Link between Microstructural and Functional Properties of Human Lateral Prefrontal Cortex. *J. Neurosci.* **41**, 2229–2244. (doi:10.1523/JNEUROSCI.2362-20.2021)

602 13. Willbrand EH *et al.* 2022 Uncovering a tripartite landmark in posterior cingulate cortex.
603   *Science Advances* **8**, eabn9516. (doi:10.1126/sciadv.abn9516)

604 14. Hathaway CB, Voorhies WI, Sathishkumar N, Mittal C, Yao JK, Miller JA, Parker BJ,
605   Weiner KS. 2023 Defining putative tertiary sulci in lateral prefrontal cortex in chimpanzees
606   using human predictions. *Brain Struct. Funct.* (doi:10.1007/s00429-023-02638-7)

607 15. Willbrand EH, Maboudian SA, Kelly JP, Parker BJ, Foster BL, Weiner KS. 2023 Sulcal
608   morphology of posteromedial cortex substantially differs between humans and
609   chimpanzees. *Communications Biology* **6**, 1–14. (doi:10.1038/s42003-023-04953-5)

610 16. Willbrand EH, Ferrer E, Bunge SA, Weiner KS. 2023 Development of human lateral
611   prefrontal sulcal morphology and its relation to reasoning performance. *J. Neurosci.*
612   (doi:10.1523/JNEUROSCI.1745-22.2023)

613 17. Voorhies WI, Miller JA, Yao JK, Bunge SA, Weiner KS. 2021 Cognitive insights from tertiary
614   sulci in prefrontal cortex. *Nat. Commun.* **12**, 5122. (doi:10.1038/s41467-021-25162-w)

615 18. Yao JK, Voorhies WI, Miller JA, Bunge SA, Weiner KS. 2022 Sulcal depth in prefrontal
616   cortex: a novel predictor of working memory performance. *Cereb. Cortex* , bhac173.
617   (doi:10.1093/cercor/bhac173)

618 19. Willbrand EH, Voorhies WI, Yao JK, Weiner KS, Bunge SA. 2022 Presence or absence of a
619   prefrontal sulcus is linked to reasoning performance during child development. *Brain Struct.*
620   *Funct.* **227**, 2543–2551. (doi:10.1007/s00429-022-02539-1)

621 20. Parker BJ *et al.* 2023 Hominoid-specific sulcal variability is related to face perception ability.
622   *Brain Struct. Funct.* (doi:10.1007/s00429-023-02611-4)

623 21. Sanides F. 1964 Structure and function of the human frontal lobe. *Neuropsychologia* **2**,
624   209–219. (doi:10.1016/0028-3932(64)90005-3)

625 22. Van Essen DC, Donahue CJ, Glasser MF. 2018 Development and Evolution of Cerebral
626   and Cerebellar Cortex. *Brain Behav. Evol.* **91**, 158–169. (doi:10.1159/000489943)

627 23. Zilles K, Palomero-Gallagher N, Amunts K. 2013 Development of cortical folding during
628   evolution and ontogeny. *Trends Neurosci.* **36**, 275–284. (doi:10.1016/j.tins.2013.01.006)

629 24. Petrides M. 2019 *Atlas of the Morphology of the Human Cerebral Cortex on the Average*
630   *MNI Brain.* Academic Press. See
631   https://play.google.com/store/books/details?id=qeWcBAAAQBAJ.

632 25. Segal E, Petrides M. 2012 The morphology and variability of the caudal rami of the superior
633   temporal sulcus. *Eur. J. Neurosci.* **36**, 2035–2053. (doi:10.1111/j.1460-9568.2012.08109.x)

634 26. Zlatkina V, Petrides M. 2014 Morphological patterns of the intraparietal sulcus and the
635   anterior intermediate parietal sulcus of Jensen in the human brain. *Proc. Biol. Sci.* **281**.
636   (doi:10.1098/rspb.2014.1493)

637 27. Drudik K, Zlatkina V, Petrides M. 2022 Morphological patterns and spatial probability maps
638   of the superior parietal sulcus in the human brain. *Cereb. Cortex*

(doi:10.1093/cercor/bhac132)

28. Goodale MA, Milner AD. 1992 Separate visual pathways for perception and action. *Trends Neurosci.* **15**, 20–25. (doi:10.1016/0166-2236(92)90344-8)

29. Humphreys GF, Tibon R. 2023 Dual-axes of functional organisation across lateral parietal cortex: the angular gyrus forms part of a multi-modal buffering system. *Brain Struct. Funct.* **228**, 341–352. (doi:10.1007/s00429-022-02510-0)

30. Harvey BM, Klein BP, Petridou N, Dumoulin SO. 2013 Topographic representation of numerosity in the human parietal cortex. *Science* **341**, 1123–1126. (doi:10.1126/science.1239052)

31. Harvey BM, Fracasso A, Petridou N, Dumoulin SO. 2015 Topographic representations of object size and relationships with numerosity reveal generalized quantity processing in human parietal cortex. *Proc. Natl. Acad. Sci. U. S. A.* **112**, 13525–13530. (doi:10.1073/pnas.1515414112)

32. Konen CS, Kastner S. 2008 Representation of eye movements and stimulus motion in topographically organized areas of human posterior parietal cortex. *J. Neurosci.* **28**, 8361–8375. (doi:10.1523/JNEUROSCI.1930-08.2008)

33. Mackey WE, Winawer J, Curtis CE. 2017 Visual field map clusters in human frontoparietal cortex. *Elife* **6**. (doi:10.7554/eLife.22974)

34. Schurz M, Tholen MG, Perner J, Mars RB, Sallet J. 2017 Specifying the brain anatomy underlying temporo-parietal junction activations for theory of mind: A review using probabilistic atlases from different imaging modalities. *Hum. Brain Mapp.* **38**, 4788–4805. (doi:10.1002/hbm.23675)

35. Tomaiuolo F, Giordano F. 2016 Cerebal sulci and gyri are intrinsic landmarks for brain navigation in individual subjects: an instrument to assist neurosurgeons in preserving cognitive function in brain tumour surgery (Commentary on Zlatkina et al.). *Eur. J. Neurosci.* **43**, 1266–1267. (doi:10.1111/ejn.13072)

36. Tomaiuolo F, Raffa G, Morelli A, Rizzo V, Germanó A, Petrides M. 2022 Sulci and gyri are topological cerebral landmarks in individual subjects: a study of brain navigation during tumour resection. *Eur. J. Neurosci.* **55**, 2037–2046. (doi:10.1111/ejn.15668)

37. Glasser MF *et al.* 2016 A multi-modal parcellation of human cerebral cortex. *Nature* **536**, 171–178. (doi:10.1038/nature18933)

38. Vendetti MS, Bunge SA. 2014 Evolutionary and developmental changes in the lateral frontoparietal network: a little goes a long way for higher-level cognition. *Neuron* **84**, 906–917. (doi:10.1016/j.neuron.2014.09.035)

39. Wendelken C. 2014 Meta-analysis: how does posterior parietal cortex contribute to reasoning? *Front. Hum. Neurosci.* **8**, 1042. (doi:10.3389/fnhum.2014.01042)

40. Karnath HO. 1997 Spatial orientation and the representation of space with parietal lobe lesions. *Philos. Trans. R. Soc. Lond. B Biol. Sci.* **352**, 1411–1419.

677   (doi:10.1098/rstb.1997.0127)

678 41. Gur RC *et al.* 2000 An fMRI study of sex differences in regional activation to a verbal and a
679   spatial task. *Brain Lang.* **74**, 157–170. (doi:10.1006/brln.2000.2325)

680 42. Dale AM, Fischl B, Sereno MI. 1999 Cortical surface-based analysis. I. Segmentation and
681   surface reconstruction. *Neuroimage* **9**, 179–194. (doi:10.1006/nimg.1998.0395)

682 43. Fischl B, Sereno MI, Dale AM. 1999 Cortical surface-based analysis. II: Inflation, flattening,
683   and a surface-based coordinate system. *Neuroimage* **9**, 195–207.
684   (doi:10.1006/nimg.1998.0396)

685 44. Glasser MF *et al.* 2013 The minimal preprocessing pipelines for the Human Connectome
686   Project. *Neuroimage* **80**, 105–124. (doi:10.1016/j.neuroimage.2013.04.127)

687 45. Barch DM *et al.* 2013 Function in the human connectome: task-fMRI and individual
688   differences in behavior. *Neuroimage* **80**, 169–189. (doi:10.1016/j.neuroimage.2013.05.033)

689 46. Roell M, Cachia A, Matejko AA, Houdé O, Ansari D, Borst G. 2021 Sulcation of the
690   intraparietal sulcus is related to symbolic but not non-symbolic number skills. *Dev. Cogn.*
691   *Neurosci.* **51**, 100998. (doi:10.1016/j.dcn.2021.100998)

692 47. Welker W. 1990 Why Does Cerebral Cortex Fissure and Fold? In *Cerebral Cortex:*
693   *Comparative Structure and Evolution of Cerebral Cortex, Part II* (eds EG Jones, A Peters),
694   pp. 3–136. Boston, MA: Springer US. (doi:10.1007/978-1-4615-3824-0_1)

695 48. Armstrong E, Schleicher A, Omran H, Curtis M, Zilles K. 1995 The ontogeny of human
696   gyrification. *Cereb. Cortex* **5**, 56–63. (doi:10.1093/cercor/5.1.56)

697 49. Chi JG, Dooling EC, Gilles FH. 1977 Gyral development of the human brain. *Ann. Neurol.*
698   **1**, 86–93. (doi:10.1002/ana.410010109)

699 50. Natu VS, Arcaro MJ, Barnett MA, Gomez J, Livingstone M, Grill-Spector K, Weiner KS.
700   2021 Sulcal Depth in the Medial Ventral Temporal Cortex Predicts the Location of a Place-
701   Selective Region in Macaques, Children, and Adults. *Cereb. Cortex* **31**, 48–61.
702   (doi:10.1093/cercor/bhaa203)

703 51. Leroy F *et al.* 2015 New human-specific brain landmark: the depth asymmetry of superior
704   temporal sulcus. *Proc. Natl. Acad. Sci. U. S. A.* **112**, 1208–1213.
705   (doi:10.1073/pnas.1412389112)

706 52. Glasser MF, Van Essen DC. 2011 Mapping human cortical areas in vivo based on myelin
707   content as revealed by T1- and T2-weighted MRI. *J. Neurosci.* **31**, 11597–11616.
708   (doi:10.1523/JNEUROSCI.2180-11.2011)

709 53. Willbrand EH, Bunge SA, Weiner KS. 2023 Neuroanatomical and functional dissociations
710   between variably present anterior lateral prefrontal sulci. *bioRxiv.* , 2023.05.25.542301.
711   (doi:10.1101/2023.05.25.542301)

712 54. Kong R *et al.* 2019 Spatial Topography of Individual-Specific Cortical Networks Predicts
713   Human Cognition, Personality, and Emotion. *Cereb. Cortex* **29**, 2533–2551.

714   (doi:10.1093/cercor/bhy123)

715   55. Heinze G, Wallisch C, Dunkler D. 2018 Variable selection - A review and recommendations
716   for the practicing statistician. *Biom. J.* **60**, 431–449. (doi:10.1002/bimj.201700067)

717   56. Dickerson BC *et al.* 2008 Detection of cortical thickness correlates of cognitive
718   performance: Reliability across MRI scan sessions, scanners, and field strengths.
719   *Neuroimage* **39**, 10–18. (doi:10.1016/j.neuroimage.2007.08.042)

720   57. Gogtay N *et al.* 2004 Dynamic mapping of human cortical development during childhood
721   through early adulthood. *Proc. Natl. Acad. Sci. U. S. A.* **101**, 8174–8179.
722   (doi:10.1073/pnas.0402680101)

723   58. Wagenmakers E-J, Farrell S. 2004 AIC model selection using Akaike weights. *Psychon.*
724   *Bull. Rev.* **11**, 192–196. (doi:10.3758/bf03206482)

725   59. Kail R, Salthouse TA. 1994 Processing speed as a mental capacity. *Acta Psychol.* **86**,
726   199–225. (doi:10.1016/0001-6918(94)90003-5)

727   60. Amunts K, Mohlberg H, Bludau S, Zilles K. 2020 Julich-Brain: A 3D probabilistic atlas of the
728   human brain's cytoarchitecture. *Science* **369**, 988–992. (doi:10.1126/science.abb4588)

729   61. Cunningham DJ. 1892 *Contribution to the Surface Anatomy of the Cerebral Hemispheres*.
730   Academy House. See https://play.google.com/store/books/details?id=t4VCAQAAIAAJ.

731   62. Wang L, Mruczek REB, Arcaro MJ, Kastner S. 2015 Probabilistic Maps of Visual
732   Topography in Human Cortex. *Cereb. Cortex* **25**, 3911–3931. (doi:10.1093/cercor/bhu277)

733   63. Benson NC *et al.* 2018 The Human Connectome Project 7 Tesla retinotopy dataset:
734   Description and population receptive field analysis. *J. Vis.* **18**, 23. (doi:10.1167/18.13.23)

735   64. Caspers S, Eickhoff SB, Rick T, von Kapri A, Kuhlen T, Huang R, Shah NJ, Zilles K. 2011
736   Probabilistic fibre tract analysis of cytoarchitectonically defined human inferior parietal
737   lobule areas reveals similarities to macaques. *Neuroimage* **58**, 362–380.
738   (doi:10.1016/j.neuroimage.2011.06.027)

739   65. Wang J, Fan L, Zhang Y, Liu Y, Jiang D, Zhang Y, Yu C, Jiang T. 2012 Tractography-
740   based parcellation of the human left inferior parietal lobule. *Neuroimage* **63**, 641–652.
741   (doi:10.1016/j.neuroimage.2012.07.045)

742   66. Reveley C, Seth AK, Pierpaoli C, Silva AC, Yu D, Saunders RC, Leopold DA, Ye FQ. 2015
743   Superficial white matter fiber systems impede detection of long-range cortical connections
744   in diffusion MR tractography. *Proc. Natl. Acad. Sci. U. S. A.* **112**, E2820–8.
745   (doi:10.1073/pnas.1418198112)

746   67. Van Essen DC, Jbabdi S, Sotiropoulos SN, Chen C, Dikranian K, Coalson T, Harwell J,
747   Behrens TEJ, Glasser MF. 2014 Mapping connections in humans and non-human
748   primates. In *Diffusion MRI*, pp. 337–358. Elsevier. (doi:10.1016/b978-0-12-396460-
749   1.00016-0)

750   68. Cottaar M, Bastiani M, Boddu N, Glasser MF, Haber S, van Essen DC, Sotiropoulos SN,

751   Jbabdi S. 2021 Modelling white matter in gyral blades as a continuous vector field.
752   *Neuroimage* **227**, 117693. (doi:10.1016/j.neuroimage.2020.117693)

753   69. Schilling K, Gao Y, Janve V, Stepniewska I, Landman BA, Anderson AW. 2018
754   Confirmation of a gyral bias in diffusion MRI fiber tractography. *Hum. Brain Mapp.* **39**,
755   1449–1466. (doi:10.1002/hbm.23936)

756   70. Schilling KG *et al.* 2023 Superficial white matter across development, young adulthood, and
757   aging: volume, thickness, and relationship with cortical features. *Brain Struct. Funct.* **228**,
758   1019–1031. (doi:10.1007/s00429-023-02642-x)

759   71. Pron A, Deruelle C, Coulon O. 2021 U-shape short-range extrinsic connectivity organisation
760   around the human central sulcus. *Brain Struct. Funct.* **226**, 179–193. (doi:10.1007/s00429-
761   020-02177-5)

762   72. Bodin C, Pron A, Le Mao M, Régis J, Belin P, Coulon O. 2021 Plis de passage in the
763   superior temporal sulcus: Morphology and local connectivity. *Neuroimage* **225**, 117513.
764   (doi:10.1016/j.neuroimage.2020.117513)

765   73. Connolly CJ. 1950 *External morphology of the primate brain*. CC Thomas.

766   74. Régis J, Mangin J-F, Ochiai T, Frouin V, Riviére D, Cachia A, Tamura M, Samson Y. 2005
767   'Sulcal Root' Generic Model: a Hypothesis to Overcome the Variability of the Human Cortex
768   Folding Patterns. *Neurol. Med. Chir.* **45**, 1–17. (doi:10.2176/nmc.45.1)

769   75. Bodin C, Takerkart S, Belin P, Coulon O. 2018 Anatomo-functional correspondence in the
770   superior temporal sulcus. *Brain Struct. Funct.* **223**, 221–232. (doi:10.1007/s00429-017-
771   1483-2)

772   76. Naselaris T, Allen E, Kay K. 2021 Extensive sampling for complete models of individual
773   brains. *Current Opinion in Behavioral Sciences* **40**, 45–51.
774   (doi:10.1016/j.cobeha.2020.12.008)

775   77. Gratton C, Nelson SM, Gordon EM. 2022 Brain-behavior correlations: Two paths toward
776   reliability. *Neuron.* **110**, 1446–1449. (doi:10.1016/j.neuron.2022.04.018)

777   78. Rosenberg MD, Finn ES. 2022 How to establish robust brain-behavior relationships without
778   thousands of individuals. *Nat. Neurosci.* **25**, 835–837. (doi:10.1038/s41593-022-01110-9)

779   79. Allen EJ *et al.* 2022 A massive 7T fMRI dataset to bridge cognitive neuroscience and
780   artificial intelligence. *Nat. Neurosci.* **25**, 116–126. (doi:10.1038/s41593-021-00962-x)

781   80. Borne L, Rivière D, Mancip M, Mangin J-F. 2020 Automatic labeling of cortical sulci using
782   patch- or CNN-based segmentation techniques combined with bottom-up geometric
783   constraints. *Med. Image Anal.* **62**, 101651. (doi:10.1016/j.media.2020.101651)

784   81. Lyu I *et al.* 2021 Labeling lateral prefrontal sulci using spherical data augmentation and
785   context-aware training. *NeuroImage.* **229**, 117758.
786   (doi:10.1016/j.neuroimage.2021.117758)